23dB On-Chip Interferometric Signal-to-Noise Enhancement via Weak Value Amplification

CNF Project Number: 2524-17

Principal Investigator(s): Jaime Cardenas

User(s): Yuhan Mei

Affiliation(s): Department of Physics and Astronomy, University of Rochester

Primary Source(s) of Research Funding: National Science Foundation Contact: jaime.cardenas@rochester.edu, ymei7@ur.rochester.edu

Research Group Website: https://www.hajim.rochester.edu/optics/cardenas/

Primary CNF Tools Used: ASML stepper, Oxford 100 Inductively coupled plasma reactive ion etching (ICP-RIE), YES EcoClean Asher, Oxford PECVD, Furnace, JEOL-9500, Woollan RC2 Spectroscopic Ellipsometer, AJA Sputter, Unaxis 770 Deep Silicon Etch, Veeco Icon AFM, PT VLN Deep Silicon Etch, Xactix Xenon Difluoride etcher

Abstract:

We demonstrate a 23dB On-chip Interferometric Signal-to-Noise Enhancement in the phase response of an on-chip weak value interferometer compared to a standard Mach-Zehnder interferometer paving the way to ultrahigh sensitivity in classical interferometry.

which offers a compact and stable solution for SNR improvement, achieving a 23dB SNR improvement that is robust against optical loss. The amplification surpasses the record 15dB tabletop quantum squeezing record to the best of our knowledge⁷.

We fabricate the device on a CMOS compatible silicon

Summary of Research:

Optical interferometry plays a critical role in precision metrology, gravitational wave detection, positioning and navigation, and environmental sensing. However, the sensitivity is fundamentally limited by quantum noises such as shot noise. Classical methods to improve the sensitivity of a measurement usually minimize electronic and technical sources of noise to operate in the shot noise limit. In this limit, the signal to noise ratio (SNR), and thus the sensitivity, can be enhanced by increasing the optical power that reaches the detector up to the point of detector saturation. Quantum strategies to improve the SNR use quantum squeezing to reduce the shot noise level, which, however, is difficult to implement in practice and very susceptible to loss.

Here, we show that weak value amplification (WVA) on a photonic chip is capable of record-breaking sensitivity enhancement by amplifying the signal without increasing the detected optical power. WVA enhances sensitivity by post-selecting photons for detection¹⁻³. WVA has previously demonstrated measurements of optical beam displacements of a few femtometers⁴ and object velocities as low as 400fm/s⁵. However, these demonstrations were shown on bulky tabletop experiments and can't access large amplifications. Previous on-chip demonstration of WVA showed an enhancement of 7dB⁶. In this work, we have successfully implemented WVA in an integrated photonic device,

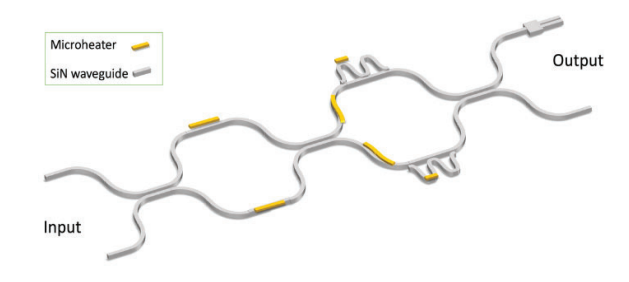


Figure 1: A schematic of A schematic of the integrated ultra-high weak value device.

nitride platform. The device schematic is given in Figure 1. The fabrication process begins by depositing a 300 nm Si3N4 layer using LPCVD on top of a 4um thermalgrown SiO2 layer as shown in Figure 2. We deposit 400nm silicon dioxide by OXFORD PECVD on top of waveguide layer as a hard mask for following etching processes. We pattern the waveguides (single mode: 1.06 um wide, multi-mode: 2 um wide) with JEOL 9500 e-beam lithography and etch with OXFORD 100. The cladding is a 2um SiO2 layer deposited by OXFORD PECVD with TEOS recipe. Next, we pattern the microheaters with ASML DUV photolithography. Then, we sputter 10 nm Titanium as an adhesion layer and another 100 nm Pt (3 um wide, 100um long) with AJA sputter. The metal residues remaining on the photoresist are then removed using acetone to finalize the formation

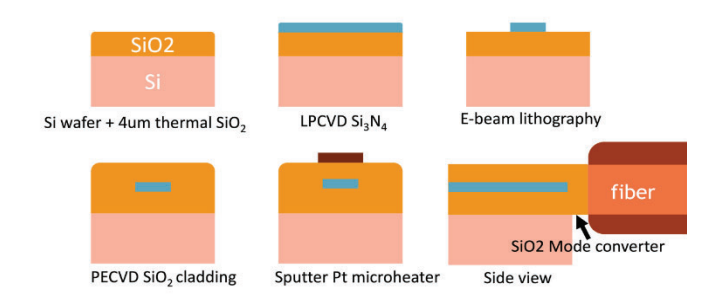


Figure 2: Main fabrication steps.

of microheaters on the chip. To improve fiber-chip coupling efficiency by matching the mode area in fiber (diameter = 10.4um), we pattern mode converters with ASML DUV photolithography at the end of inversed waveguide tapers (short sections of SiO2 measuring 10um in length and tapering from 20um to 11.5um in width suspended in the air). 8,9We etch 6 um SiO2 with OXFORD 100 and then etch Si by 160um with Bosch process with VLN deep Silicon etcher. Finally, we undercut the silicon under the mode converter consist of silicon dioxide with Xactix Xenon Difluoride (XeF2) etcher.

Conclusions and Future Steps:

We have successfully tested 23dB SNR improvement by weak value amplification in fabricated integrated photonic devices. Our future research aims to apply this technique to capture phase signals from external information carriers, such as making a highly sensitive gyroscope.

- [1] Aharonov, Y. How the result of a measurement of a component of the spin of a spin-1/2 particle can turn out to be 100. Phys. Rev. Lett. 60, 1351–1354 (1988).
- [2] Duck, I. M., Stevenson, P. M. & Sudarshan, E. C. G. The sense in which a 'weak measurement' of a spin-½ particle's spin component yields a value 100. Phys. Rev. D 40, 2112–2117 (1989).
- [3] Dressel, J., Malik, M., Miatto, F. M., Jordan, A. N. & Boyd, R. W. Colloquium: Understanding quantum weak values: Basics and applications. Rev. Mod. Phys. 86, 307–316 (2014).
- [4] Dixon, P. B., Starling, D. J., Jordan, A. N. & Howell, J. C. Ultrasensitive Beam Deflection Measurement via Interferometric Weak Value Amplification. Phys. Rev. Lett. 102, 173601 (2009).
- [5] Viza, G. I. et al. Weak-values technique for velocity measurements. Optics Letters 38, 2949–2952 (2013).
- [6] Song, M. et al. Enhanced on-chip phase measurement by inverse weak value amplification. Nat Commun 12, 6247 (2021).
- [7] Vahlbruch, H., Mehmet, M., Danzmann, K. & Schnabel, R. Detection of 15 dB Squeezed States of Light and their Application for the Absolute Calibration of Photoelectric Quantum Efficiency. Phys. Rev. Lett. 117, 110801 (2016).
- [8] Nauriyal, J., Song, M., Yu, R. & Cardenas, J. Fiber-to-chip fusion splicing for low-loss photonic packaging. Optica, OPTICA 6, 549–552 (2019).
- [9] Kumar, S., Nauriyal, J. & Cardenas, J. Low-Loss, High Extinction Ratio Fiber to Chip Connection via Laser Fusion for Polarization Maintaining Fibers. in 2023 Optical Fiber Communications Conference and Exhibition (OFC) 1–3 (2023). doi:10.1364/OFC.2023.M3C.1.

On-Chip Soliton Generation

CNF Project Number: 2524-17

Principal Investigator(s): Jaime Cardenas User(s): Arunima Nauriyal and Sushant Kumar

Affiliation(s): University of Rochester, Institute of Optics

Contact: jaime.cardenas@rochester.edu, anauriya@ur.rochester.edu Primary CNF Tools Used: PECVD, LPCVD Furnace, Electron beam

lithography JEOL 9500, ASML, Oxford 100, Unaxis, dicing saw, Piranha, YES eco clean

Abstract:

Development of on chip soliton generation using dispersion management. Carefully designing the waveguides by manipulating the dispersion properties of silicon nitride. Improving fiber to chip coupling efficiency by integrating mode converters [Fig. 1] to improve on chip soliton properties.

Summary of Research:

We achieved our goal of getting high energy anomalous dispersion soliton on chip. For a smoother surface we deposited TEOS using PECVD followed by the twist and grow method [1] in E4 furnace for LPCVD of thick nitride to manage nitride stress. Double pass writing was used in JEOL 9500 for higher precision and O factor. To ensure we have no air gaps between the ring resonator and the bus waveguide we deposit HTO in furnace followed by TEOS deposition in PECVD as the upper cladding. The next step was using ASML lithography to pattern mode converters [2] on our wafer to maximize chips to fiber coupling. Etching oxide and nitride layers were done using the OXFORD 100 standard recipes. Silicon etching was performed using the Unaxis as Versaline was down, this was then followed by undercutting the wafer using Xenon difluoride. Many of these devices are under testing so we do not have results on the device performance yet.

Conclusions and Future Steps:

Our novel method for generation of solitons on chips was carefully and successfully implemented by using the tool available to us by CNF. We will be working on improving the devices to achieve higher peak power solitons and help the academic industry grow in knowledge.



Figure 1: Mode converter Top view

Acknowledgements:

The authors wish to thank National Science Foundation funding (award CCF-1918549). PLM gratefully acknowledges financial support from a David and Lucile Packard Foundation Fellowship. The authors wish to thank NTT Research for their financial and technical support. We gratefully acknowledge the Air Force Office of Scientific Research for funding under Award Number FA9550-22-1-0378. This work was performed in part at the Cornell NanoScale Facility, a member of the NNCI, which is supported by NSF Grant NNCI-2025233.

- [1] Houssein El Dirani, Laurene Youssef, Camille Petit-Etienne, Sebastien Kerdiles, Philippe Grosse, Christelle Monat, Erwine Pargon, and Corrado Sciancalepore,,""Ultralow-loss tightly confining Si3N4 waveguides and high-Q microresonators,"," in Opt. Express 27, 30726-30740 (2019).
- [2] Juniyali Nauriyal, Meiting Song, Yi Zhang, Marissa Granados-Baez, and Jaime Cardenas, ""Fiber array to chip attach using laser fusion splicing for low loss"," Opt. Express 31, 21863-21869 (2023).

Suspended Multimode SiN Platform for Strong Intermodal Brillouin Scattering

CNF Project Number: 2524-17

Principal Investigator(s): Jaime Cardenas

User(s): Jiewei Xiang

Affiliation(s): The Institute of Optics, University of Rochester

Contact: jaime.cardenas@rochester.edu, jxiang6@ur.rochester.edu

Primary CNF Tools Used: ASML stepper, Oxford 100 Inductively coupled plasma reactive ion etching (ICP-RIE), YES EcoClean Asher, Oxford PECVD, Furnace, JEOL-9500, Heidelberg Mask Writer-DWL2000, ABM Contact Aligner, Woollan RC2 Spectroscopic Ellipsometer, YES Ecoclean asher, Critical pointer dryer-Leica

Abstract:

We demonstrate forward intermodal Brillouin interactions with fundamental acoustic modes (FIM-FAM) in a suspended triple-core Si₃N₄ waveguide, achieving sub-50 kHz linewidths and a gain coefficient over 1100 W⁻¹·m⁻¹. This platform enables narrowband RF filtering in a CMOS-compatible photonic circuit.

Summary of Research:

Microwave filters based on stimulated Brillouin scattering (SBS) in integrated photonic platforms offer the potential for ultra-narrowband, reconfigurable RF filtering with high spectral resolution and compact form factors¹⁻⁴. While Brillouin interactions in silicon nitride (Si₂N₄) waveguides are attractive due to the material's low optical loss and CMOS compatibility, achieving high SBS gain has been hindered by low photoelasticity and weak acoustic confinement⁵⁻⁷. To overcome these challenges, we demonstrate an on-chip forward intermodal SBS platform based on a suspended triple-core Si₃N₄ waveguide structure. This design supports SBS interactions between the TE₁ and TM₀ optical modes, which collectively drive low-frequency fundamental acoustic modes, including both flexural-y and torsional modes, via radiation pressure.

The waveguide geometry is carefully optimized to

support strong acoustic mode confinement through large impedance mismatch at air-Si₃N₄ interface and to ensure momentum matching by engineering the effective index difference between the interacting optical modes. Importantly, the suspended waveguide is fabricated with a central core and two symmetric outer cores, creating a spatially distributed radiation pressure profile that avoids destructive cancellation and enhances net optical force coupling.

Using phonon-mediated four-wave mixing spectroscopy, we measure a Brillouin gain coefficient exceeding 1100 W⁻¹·m⁻¹ and linewidths as low as 45 kHz, representing a record performance for SBS in Si₃N₄ waveguides. The suspended region is defined using a combination of dry etching and buffered oxide undercut, followed by critical point drying to preserve mechanical integrity. The triplecore waveguide supports large acoustic impedance mismatch with the surrounding air, suppressing phonon leakage and maintaining long phonon lifetimes. The structure also enables the formation of an acoustic cavity, where coherent reflections at the suspended region boundaries discretize the phonon spectrum, contributing to reduced acoustic linewidth.

This platform provides efficient access to fundamental acoustic modes with long coherence times and enables RF filtering capabilities that are fully compatible with planar photonic integration. Compared to SBS in

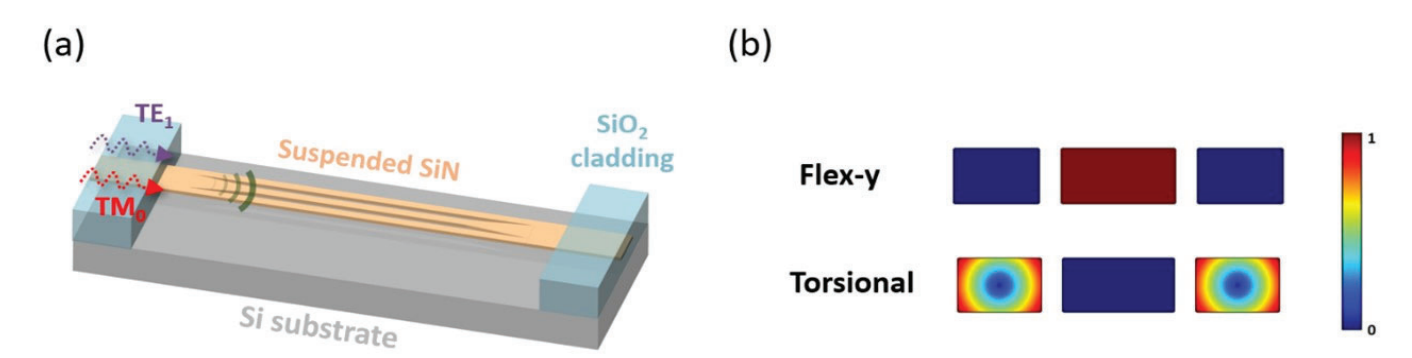


Figure 1: (a) Schematic of the suspended triple waveguide design (b) Simulated results for flexural-y and torsional acoustic modes.

optical fibers or hybrid materials, the demonstrated approach offers significant size reduction and process scalability, laying the foundation for on-chip microwave photonic filters with kHz-level resolution, high spectral selectivity, and low power operation.

Schematic plot of the suspended triple waveguide design and two fundamental acoustic modes confined in triple-core waveguide are shown in Fig. 1. The main fabrication steps for our design are illustrated in Fig. 2. The fabrication process begins with the deposition of a 4 µm thermal oxide bottom cladding layer, followed by a low-loss silicon nitride (Si₂N₄) core layer using low-pressure chemical vapor deposition (LPCVD). A PECVD oxide layer is then deposited to serve as an etch mask. Waveguides are defined using electron-beam lithography with a JEOL-9500 system and a negativetone MaN resist. The pattern is transferred into the Si₂N₄ layer via inductively coupled plasma reactive ion etching (ICP-RIE) using an Oxford 100 system. Post-etching, the resist is stripped with a YES EcoClean plasma asher, and a top oxide cladding is deposited using PECVD.

To define the suspended region, a protective GKR resist layer is spun onto the chip, and an ASML stepper is used to expose the undercut windows. The top oxide thickness in the suspended area is partially reduced by another ICP etching step using the Oxford 100. The chip is then immersed in buffered oxide etchant (BOE) to selectively undercut the oxide beneath the waveguides, thereby achieving full suspension of the Si₃N₄ core. Finally, a critical point dryer (Leica CPD) is used to ensure structural integrity during the drying process. Fig. 3 shows the SEM image of the suspended Si₃N₄ waveguide, drying with the nitrogen gun and the critical point dryer.

Conclusions and Future Steps:

In conclusion, we demonstrate efficient on-chip forward intermodal stimulated Brillouin scattering (SBS) in a suspended triple-core silicon nitride waveguide, enabling strong interaction with low-frequency fundamental acoustic modes. Through careful mode engineering and acoustic confinement, we achieve a record Brillouin gain coefficient exceeding 1100 W⁻¹·m⁻¹ with sub-50 kHz linewidths. This platform offers a compact, CMOS-compatible solution for narrowband microwave photonic filtering and establishes a scalable foundation for future low-power, high-resolution RF signal processing on chip.

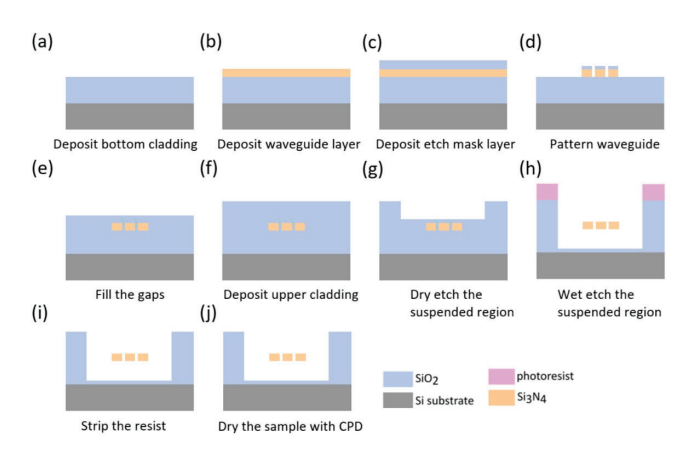


Figure 2: The main fabrication steps.

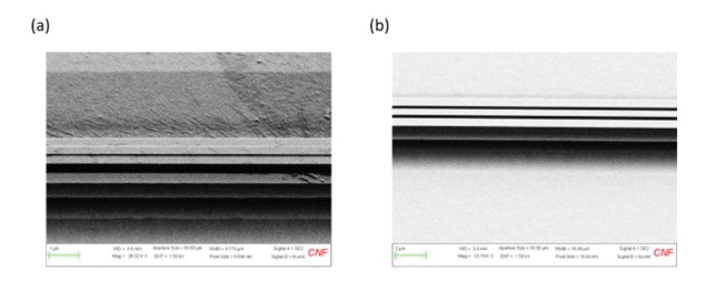


Figure 3: The SEM pictures of suspended Si3N4 waveguide. (a) Drying with the nitrogen gun (b) Drying with the critical point dryer.

- Liu, Y. et al. Integration of Brillouin and passive circuits for enhanced radio-frequency photonic filtering. APL Photonics 4, 106103 (2019).
- [2] Choudhary, A., Liu, Y., Marpaung, D. & Eggleton, B. J. On-Chip Brillouin Filtering of RF and Optical Signals. IEEE J. Sel. Top. Quantum Electron. 24, 1–11 (2018).
- [3] Marpaung, D. et al. Low-power, chip-based stimulated Brillouin scattering microwave photonic filter with ultrahigh selectivity. Optica 2, 76–83 (2015).
- [4] Eggleton, B. J., Poulton, C. G., Rakich, P. T., Steel, Michael. J. & Bahl, G. Brillouin integrated photonics. Nat. Photonics 13, 664–677 (2019).
- [5] Klaver, Y. et al. Surface acoustic waves Brillouin photonics on a silicon nitride chip. Preprint at http://arxiv.org/ abs/2410.16263 (2024).
- [6] Botter, R. et al. Guided-acoustic stimulated Brillouin scattering in silicon nitride photonic circuits. Sci. Adv. 8, eabq2196 (2022).
- [7] Gyger, F. et al. Observation of Stimulated Brillouin Scattering in Silicon Nitride Integrated Waveguides. Phys. Rev. Lett. 124, 013902 (2020).

Reducing the Operating Voltage of Deep-Ultraviolet Light Emitting Diodes

CNF Project Number: 2801-19

Principal Investigator(s): Debdeep Jena and Huili (Grace) Xing

User(s): Sheena (Hsin Wei) Huang

Affiliation(s): Electrical and Computer Engineering, Cornell University

Primary Source(s) of Research Funding: DARPA Contact: djena@cornell.edu, hh494@cornell.edu

Research Group Website: https://jena-xing.engineering.cornell.edu/

Primary CNF Tools Used: PT770 ICP-RIE, Oxford PE-ALD, E-beam evaporator, AS 200 I-line stepper, Heidelberg

MLA, Ultra SEM, PE-CVD, Woollam RC2 ellipsometer

Abstract:

Improving the electrical efficiency of deep-ultraviolet light emitting diodes (DUV- LEDs) based on the ultrawide bandgap material AlGaN is important for applications in disinfection, sensing, and lithography. Reducing the contact resistance of the device is crucial to improving the electrical efficiency. For high-performance electronic and optoelectronic devices, specific contact resistivities (p_c) on the order of 10^{-5} - 10^{-6} Ωcm^2 are typically required. However, the ultrawide bandgap nature of AlGaN alloys poses intrinsic difficulties in achieving such low-resistance contacts. In this study, we investigate the co- optimization of p-InGaN and n-AlGaN contacts of DUV LEDs in monolithic integration.

These diodes are grown pseudomorphically on bulk AlN substrates by molecular beam epitaxy (MBE), resulting in low threading dislocation density and allowing for internal quantum efficiency (IQE), carrier injection efficiency (CIE), and lifetime of devices. The goal of this work is towards an electrically-injected DUV laser

diode grown by MBE.

Summary of Research:

We find that using a thin $In_{0.07}Ga_{0.93}N$ cap is effective in achieving ohmic p-contacts with specific contact resistivity of $3.10\times10^{-5}~\Omega cm^2$. Upon monolithic integration of p- and n-contacts for DUV LEDs, we find that the high temperature annealing of 800 °C required for the formation of low resistance contacts to n-AlGaN severely degrades the p-InGaN layer, thereby reducing the hole concentration and increasing the specific contact resistivity to $9.72\times10^{-4}~\Omega cm^2$. Depositing a SiO₂ cap by plasma-enhanced atomic layer deposition (PE-ALD) prior to high temperature n-contact annealing restores the low p-contact resistivity, enabling simultaneous low-resistance p- and n-contacts.

DUV-LEDs emitting at 268 nm fabricated with the SiO_2 technique exhibit a 3.5 V reduction in operating voltage at a current level of 400 A/cm² and 1.9 m Ω cm² decrease in differential ON-resistance. This study highlights a

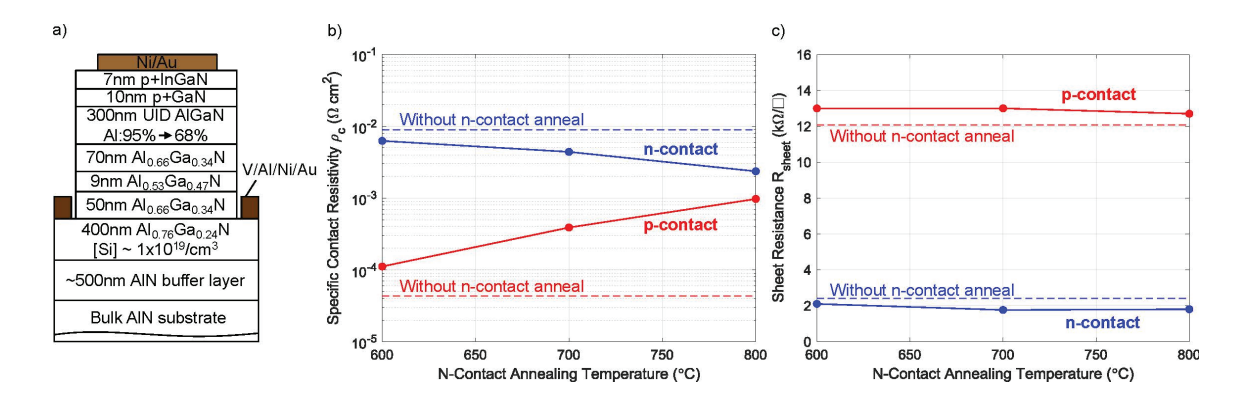


Figure 1: (a) Heterostructure of the DUV LED samples used for this contact annealing temperature-dependent study. (b) Specific contact resistivity of n- and p-contact vs n- contact annealing temperature. P-contacts were subsequently annealed at 450 °C. All resistance values were extracted at 1 mA from CTLM-IV measurement. (c) Sheet resistance vs n-contact annealing temperature.

scalable route to high-performance, high-Al-content bipolar AlGaN devices.

Conclusions and Future Steps:

We are continuing to reduce the contact resistance of the p- and n-contacts through different metallization annealing conditions, metal stack, and acid treatment. We would also like to experiment with different capping materials like SiN and AlN to further reduce the degradation of p-InGaN during n-contact anneal.

- [1] Appl. Phys. Express 12, 124003 (2019)
- [2] Advanced Electronic Materials 11, 2300840 (2025)
- [3] Applied Physics Letters 124, 102109 (2024)

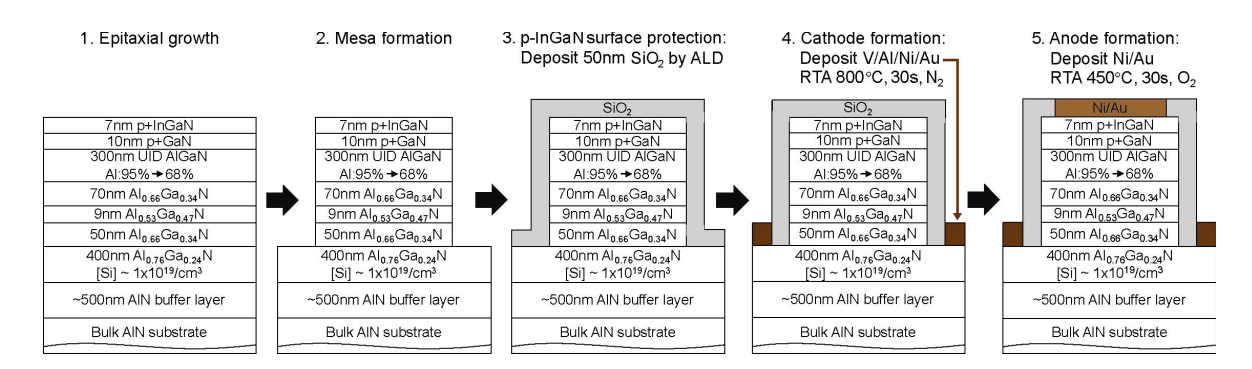


Figure 2: Schematic diagram illustrating the fabrication process of an LED with the SiO2 capping technique.

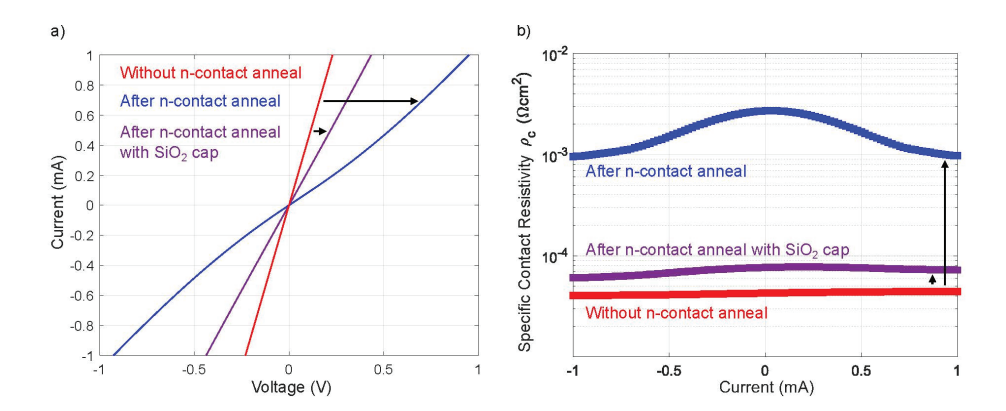


Figure 3: (a) CTLM-IV curves comparison of p-contact without undergoing n contact anneal, after undergoing n-contact anneal with SiO2 cap, and after undergoing n-contact anneal without SiO2 cap. IVs are plotted for 2 µm spacing. (b) Resistance vs metal electrode spacings for the data shown in (a).

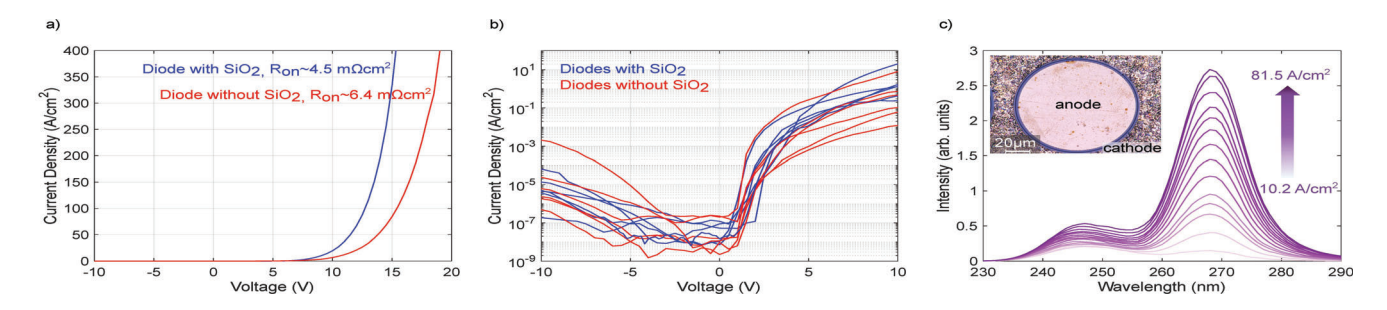


Figure 4: (a) Room temperature J-V characteristics of two LEDs, one with SiO2 capping method and one without. The differential ON- resistance was extracted at 400A/cm2. (b) IV from batch test of LEDs with and without SiO2 capping. (c) Room temperature electroluminescence of an LED with the SiO2 capping method. Inset shows the microscopy image of a fabricated LED.

Towards Release-Free Intermodal Acousto-Optic Modulation at Visible and UV Wavelengths

CNF Project Number: 2985-21

Principal Investigator(s): Karan Kartik Mehta (2)

User(s): Oscar Jaramillo(1, 2)

Affiliation(s): School of Applied and Engineering Physics, Cornell University (2) School of Electrical and Computer Engineering, Cornell University

Primary Source(s) of Research Funding: NSF

Contact: karanmehta@cornell.edu, oj43@cornell.edu

Primary CNF Tools Used: Zeiss Ultra SEM, PT770 Etcher, Woollam RC2 Spectroscopic Ellipsometer, SC4500 Evaporator, Oxford PECVD, Keyence VHX-7100 Digital Microscope, Oxford FlexAL, OEM Endeavor M1, ASML Stepper

Abstract:

We present an inter-modal acousto-optic modulator designed to operate near $\lambda \sim 405$ nm, leveraging acoustic modes confined and co-localized with a buried optical waveguide. We demonstrate the acoustic waveguiding concept, predicted to enable opto-mechanical coupling coefficient $g \approx 2 \text{ (sqrt(μW)mm)}^{-1}$.

Summary of Research, 2023-2024 Progress:

Acousto-optic modulators (AOMs) are widely used for frequency, phase, and amplitude control in a broad range of applications. Tabletop systems suffer from a relatively large footprint since the acoustic power is delocalized relative to the optical power. As a result, they typically consume on the order of 1-10 Watts, limiting their scalability and compatibility with multiplexed on-chip systems. Promising efficiencies of on-chip AOMs

have been demonstrated at $\lambda \sim 780\text{-}1550$ nm^[1-4]. In certain cases, the use of non-standard CMOS materials and/or the fabrication complexity—such as released structures—pose challenges for large-scale integration. Furthermore, the materials employed to date are lossy in the UV and visible, essential for a variety of applications such as bio-chemical spectroscopy, and quantum control of trapped ions, neutral atoms, and solid-state quantum systems ^[5,6].

We present a design for robust, low-power, compact, and CMOS-compatible on-chip AOMs in the blue and UV, and demonstrate the fundamental waveguiding principle in our concept, towards scalable modulation for atomic systems. The concept leverages the high refractive index (RI) contrast offered by HfO2-Al2O3 composites $^{[7]}$, resulting in high opto-mechanical coupling coefficient g owing to 3 scaling from photoelasticity and $\sim \epsilon^2 (\epsilon \text{clad}^{-1} - \epsilon \text{core}^{-1})$ core from waveguide boundary movement $^{[1]}$.

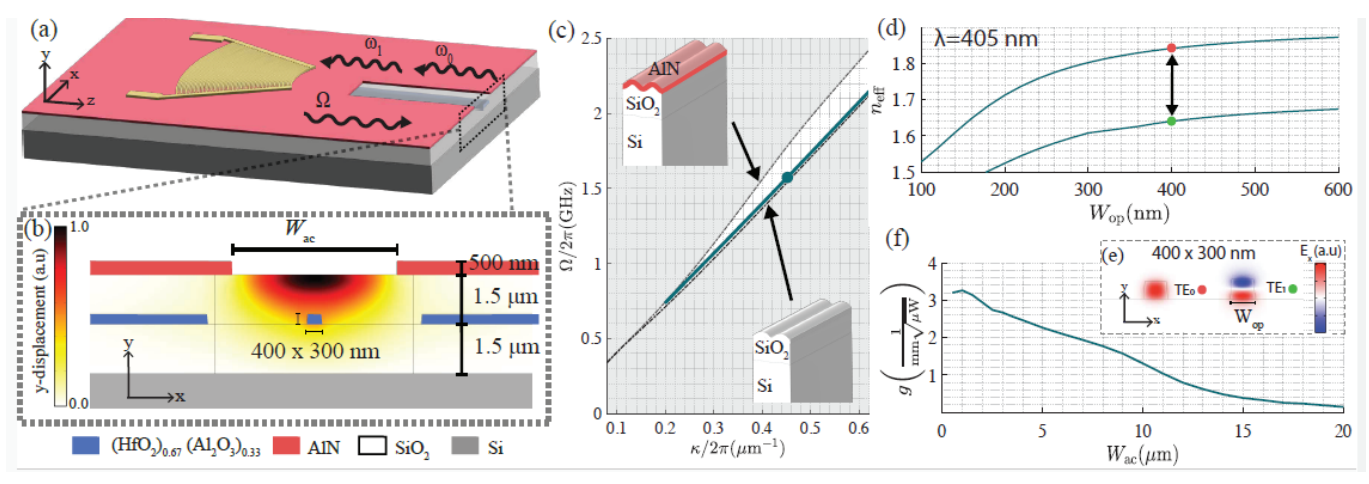


Figure 1: a) Schematic of a release-free AOM with co-confined acoustic and optical modes. (b) Cross section showing the dominant (y) displacement of a confined acoustic mode. c) Dispersion of guided mode with top (bottom) light-cone of a AlN+SiO₂ (SiO₂) RM. d) Effective index $n_{\rm eff}$ of optical modes vs optical waveguide width $W_{\rm op}$ with points representing modes used to calculate g. Gray modes are the non phase-matched modes. f) Simulated g for a 400 ×300 nm optical waveguide vs acoustic waveguide width ($W_{\rm ae}$). Use of buried optical waveguides facilitates integration in CMOS- like stacks, along with integration of additional photonic waveguide layers for mode demultiplexing.

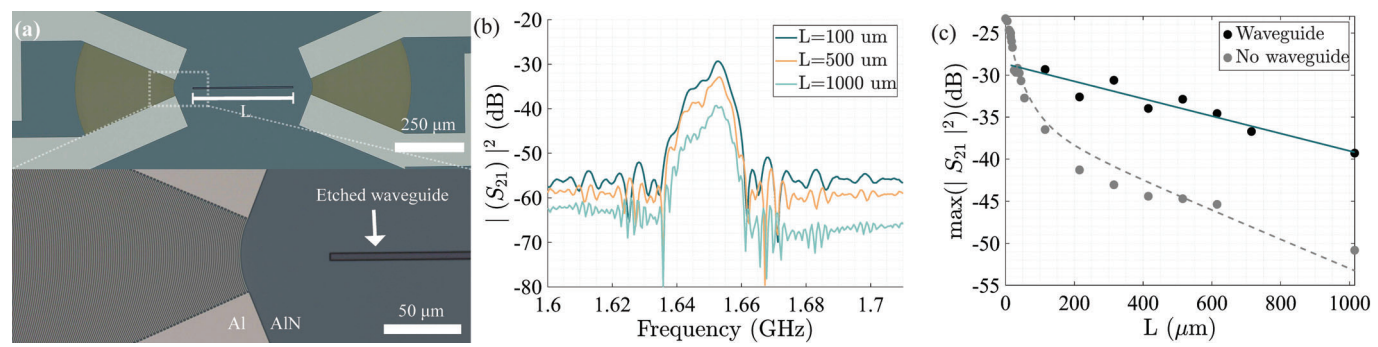


Figure 2: . a) Micrograph of a fabricated device with acoustic waveguide length L. b) Subset of representative |S12 | 2 curves. c) Peak values for |S12|2 vs L for structures without and with the acoustic waveguide etched, indicating clear acoustic guiding.

Our AOM is composed of a (HfO₂)₆₇(Al2O₃)₆₇ multimode optical-waveguide buried in SiO2 and a 500 nm thick film of sputtered AlN used to launch a counterpropagating acoustic wave via a focusing inter-digitated transducer (Fig. 1a). The overall film stackup supports a RM (top inset of Fig. 1c), which together with an etched trench of width W_{ac} on AlN, creates a confined acoustic mode that overlaps with the buried optical waveguide (Fig. 1b). This mode is characterized by its dominant displacement along the y- direction, which shifts the top and bottom boundaries of the optical mode, coupling the TE₀ and the TE₁ modes at $\lambda = 405$ nm (Fig. 1d). As W decreases, the acoustic energy overlap with the waveguide increases, resulting in a higher g. The acoustic wave induces oscillations in power between the optical modes, achieving full conversion from the TE₀ to the TE₁ mode at an acoustic power of $P_{\pi/2} = (\pi/(2gL_{\text{eff}}))^2$, where $L_{\rm eff} = (1 - \exp(-\alpha_{\rm wg} L))/\alpha_{\rm wg}$ is the effective length and $\alpha_{\rm wg}$ is the acoustic waveguide loss.

To demonstrate the acoustic guiding principle, we design and fabricate the device from Fig. 1a without the optical waveguide. We sputter ~500 nm of AlN on 3 um of thermal SiO2, pattern the electrodes with 100 nm of aluminum using a lift-off process and etch the waveguide with a dry etch process. A fabricated device with acoustic waveguide length L= 500 μm is shown in Fig. 2a. To estimate propagation loss ignoring reflections, we measure S21 for L varying from 100 to 1000 µm (Fig. 2b) and take the peak value as the transmission (Fig. 2c). A fit to $max(|S_{12}|^2) = \eta^2 exp(-1)$ $\alpha_{_{\!\scriptscriptstyle \mathsf{U\!\!\!\!U}\!\!\scriptscriptstyle o}} L)$ indicates a transducer-WG coupling efficiency $|\eta| = -14.4 \pm 0.4 \text{ dB}$ and $\alpha_{wg} = 10.3 \pm 1.6 \text{ dB/mm}$. Fig 2c also shows measurements of the same device prior to trench etching, demonstrating that as L increases, the transmission follows our model, which accounts for losses due to mode mismatch from defocusing, along with a Rayleigh-mode (RM) loss of approximately αRM ~9 dB/mm. With the etched waveguide, the transmission remains linear for an etched waveguide, indicating the functioning of the acoustic guiding. The measured

transduction efficiency and acoustic waveguide loss project that a device with the $(HfO_2)_{.67}(Al_2O_3)_{.33}$ film should exhibit full mode-conversion in L= 100 μ m with an RF driving power below 2.5 mW.

This work establishes an efficient platform for onchip inter-modal acousto-optic modulation in a CMOS compatible and release-free configuration at blue and UV wavelengths. Realization of the full acousto-optic device leveraging the demonstrated optical and acoustic waveguides and transducers together is in progress. This platform may enable foundry-compatible efficient active control of UV and visible light in integrated systems.

- [1] C. J. Sarabalis et al., "Acousto-optic modulation of a wavelength-scale waveguide," Optica 8, 477–483 (2021).
- [2] L. Zhang et al., "Integrated-waveguide-based acousto-optic modulation with complete optical conversion," Optica 11, 184–189 (2024).
- [3] E. A. Kittlaus et al., "Electrically driven acousto-optics and broadband non-reciprocity in silicon photonics," Nat. Photonics 15, 43–52 (2021).
- [4] Q. Lin et al., "Optical multi-beam steering and communication using integrated acousto-optics arrays," Nat. Commun. 16, 1–7 (2025).
- [5] D. J. Blumenthal, "Photonic integration for UV to IR applications," APL Photonics 5 (2020).
- [6] G. Moody et al., "2022 roadmap on integrated quantum photonics," J. Phys.: Photonics 4, 012501 (2022).
- [7] O. Jaramillo et al., "HfO₂-based platform for high-indexcontrast visible and UV integrated photonics," Opt. Lett. 50, 3165–3168 (2025).

Programmable Poling for Electric Field Induced Second Harmonic Generation

CNF Project Number: 2971-21

Principal Investigator(s): Peter McMahon [1, 2]

User(s): Ryotatsu Yanagimoto [1, 3], Benjamin Ash [1, 3], Yiqi Zhao [1, 3]

Affiliation(s): [1] School of Applied and Engineering Physics, Cornell University, Ithaca, NY 14853, USA; [2] Kavli Institute at Cornell for Nanoscale Science, Cornell University, Ithaca, NY 14853, USA; [3] NTT Physics and Informatics Laboratories, NTT Research, Inc., Sunnyvale, CA, USA

Primary Source(s) of Research Funding: National Science Foundation (award CCF-1918549) PLM gratefully acknowledges financial support from a David and Lucile Packard Foundation Fellowship. The authors wish to thank NTT Research for their financial and technical support. We gratefully acknowledge the Air Force Office of Scientific Research for funding under Award Number FA9550-22-1-0378. This work was performed in part at the Cornell NanoScale Facility, a member of the National Nanotechnology Coordinated Infrastructure (NNCI), which is supported by the National Science Foundation (Grant NNCI-2025233)

Contact: pmcmahon@cornell.edu, ry338@cornell.edu, baa77@cornell.edu, yz2893@cornell.edu Primary CNF Tools Used: Oxford PECVD, Oxford 100 ICP Dielectric, ASML DUV Stepper

Abstract:

Nonlinear photonics uses coherent interactions between optical waves to engineer functionality that is not possible with purely linear optics. Traditionally, the function of a nonlinear-optical device is determined during design and fixed during fabrication, which limits the scope and flexibility of its use. Here, we present a photonic device with an arbitrarily reconfigurable distribution of $\chi^{(2)}$ nonlinearity. To showcase the versatility of our device, we demonstrated spectral, spatial, and spatio-spectral engineering of second-harmonic generation by tailoring the quasi-phase-matching (QPM) grating structures in a two dimensional slab waveguied. Moreover, we have demonstrated record-breaking on-chip poling lengths by optimizing our poling pattern to a spiral waveguide geometry. Our work shows that we can transcend the conventional one-device-one-function paradigm, expanding the potential applications of nonlinear optics in situations where fast device reconfigurability is not merely practically convenient but essential—such as in programmable optical quantum gates and quantum light sources, all-optical signal processing, optical computation, and adaptive structured light for sensing.

Summary of Research:

Lithography-free photonics has attracted considerable attention in the field of programmable photonics because the large number of programmable parameters allows the device to move beyond the one-device—one-function paradigm. This means lithography-free devices can perform a large range of tasks and compensate for fabrication error [1]. Recent advances in lithography-free technology have enabled a device with real index

of refraction modulation on-chip. In this device, a photoconductor and waveguiding layer with high native $\chi^{(2)}$ nonlinearity are stacked in series and placed under high voltage, allowing the two layers act as a voltage divider. Because the index of refraction of the waveguiding layer depends on the electric bias, the index of refraction can be spatially controlled by shining different patterns of light onto the photoconductor [2]. Using the same device concept, the core material can be replaced with silicon nitride, which possesses a large induced $\chi^{(2)}$ during an electric-field induced second harmonic (E-Fish) process.

By engineering $\chi^{(2)}$ quasi-phase matching (QPM) gratings on a two-dimensional slab waveguide, we realized versatile functions on a single device, flexibly controlling nonlinear- optical processes in the spectral, spatial, and spatio-spectral domains. The programmability of the device further enabled in-situ inverse designs and optimizations based on real-time experimental feedback, robustly achieving complex functions that are challenging on conventional nonprogrammable devices [3]. This approach can be extended to one-dimensional channel waveguide, where the loss of orthogonal spatial programmability is compensated by lower propagation loss, broader band operation, and longer interaction length. Preliminary studies show super-linear scaling of the nonlinear conversion efficiency with increased interaction length, paving a way for programmable nonlinear photonics on silicon nitride to one day rival lithium niobate.

Spatio-Spectral Engineering on Programmable Slab Waveguide:

To fabricate the nonlinear programmable slab waveguide, we started with a conductive P- type doped Si substrate

with 1 μ m of thermal SiO₂ and 2 μ m of PECVD SiN_x provided by Silicon Valley Microelectronics. We then deposit 1 μ m of PECVD SiO₂ followed by 12 μ m of PECVD silicon-rich nitride (SRN), which acts as the photoconductive layer in the device.

Lastly, we sputter 30 nm of indium tin oxide (ITO) as our top electrode. After cleaving and polishing the waveguide facet, we couple an ELMO-HP pulsed laser from Menlo systems into the waveguide, apply high voltage to the stack, and project an image (generated by a spatial light modulator) onto device. The photoconductor and waveguide layers act as a voltage divider, so whenever the photoconductor becomes more conductive upon illumination, more voltage drops in the waveguiding layer, inducing a larger $\chi^{(2)}$ nonlinearity in the illuminated region. This process is shown in figure 1. The output of the waveguide is then imaged out to a grating, which separates the spectral components of each spatial position.

By sculpting the spatial $\chi^{(2)}(x, z)$ pattern, we can programmably phase match different processes at once. As figure 1 shows, we can engineer the output second harmonic wavefront in both the spatial and spectral domain by reprogramming the $\chi^{(2)}(x, z)$ pattern. Furthermore, because we can alter the nonlinearity distribution with no memory of the previous pattern, we can optimize the poling pattern to produce non-trivial spectral outputs. Figure 2 shows this concept, where we can use analytic poling patterns to produce easy spectral outputs, but more complicated outputs rely upon real-time feedback and optimization.

Super-linear Conversion Efficiency Scaling on Programmable Channel Waveguide:

Using the same principle as the slab waveguide, we fabricated a programmable channel waveguide using SiNx. To fabricate this device, we start with a conductive P-type doped Si substrate with 1 µm of thermal SiO₂. We then deposit 2 µm of PECVD SiNx and etch it using a CHF₃/O₂/N₂ chemistry and SiO₂ hard mask. We deposit an additional 1 µm of conformal PECVD SiO₂ followed by a 4 hour 1200 °C anneal to drive N-H bonds out of the film. We then follow the same process as the slab waveguide, depositing 12 µm of PECVD (SRN), sputtering, 30 nm of ITO, and cleaving the facets open.

With a finished device, we couple a Santec TSL-570 continuous-wave laser into a spiral structure and pole along the outer Archimedes spiral waveguide. By utilizing interference between different subdivisions of the spiral, the phase and poling period of each section can be optimized to achieve superliner scaling. Figure 3 shows the scaling of SHG signal measured with increasing poling distance (measured on a

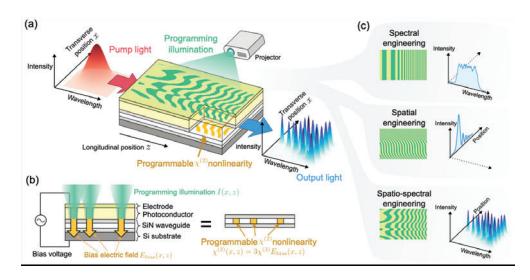


Figure 1: Overview of spatio-spectral engineering. a) Device operational overview. b) Schematic of how programmable illumination induces a programmable $\chi(2)$ nonlinearity. c) Experimental data showing how different programmed poling periods yield different beam outputs in the spatial and spectral domain,

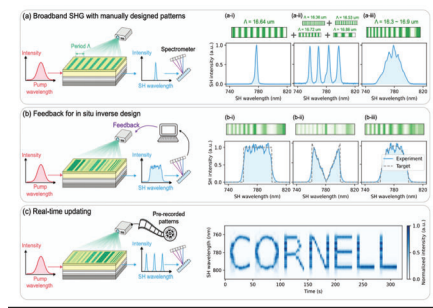


Figure 2: Real-time optimization of poling pattern. a) Output spectra from a single poling period, multiple poling periods added, and a chirped poling period. b) Different output spectra achieved through real-time optimization of the poling period. c) Output spectra changing in time to print the word "CORNELL".

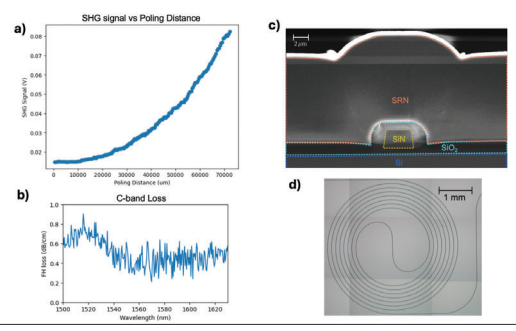


Figure 3: Early results on programmable channel waveguides. a) Super linear scaling of the second harmonic signal, as measured on a photomultiplier tube. The signal scaled with poling distance to the power of 2.5 and poling was done over a total of 7 cm. b) Loss measurement on device using cut-back method. c) SEM image of device cross-section with each material layer labeled. d) Microscope image of a device with a 7 cm spiral.

photomultiplier tube) and the loss of the device over the C-band, which shows the broadband potential of this device to be reprogrammed for efficient conversion.

- [1] P. L. McMahon, Nature Reviews Physics 5, 717 (2023).
- [2] T. Onodera, M. M. Stein, B. A. Ash, M. M. Sohoni, M. Bosch, R. Yanagimoto, M. Jankowski, T. P.McKenna, T. Wang, G. Shvets, M. R. Shcherbakov, L. G. Wright, and P. L. McMahon, Scaling on-chip photonic neural processors using arbitrarily programmable wave propagation (2024), arXiv:2402.17750
- [3] Ryotatsu Yanagimoto, Benjamin A Ash, Mandar M Sohoni, Martin M Stein, Yiqi Zhao, Federico Presutti, Marc Jankowski, Logan G Wright, Tatsuhiro Onodera, Peter L McMahon, Programmable on-chip nonlinear photonics (2025), arXiv:2503.19861

Photonic Integrated Technologies for Low-SWaP, Narrow- Linewidth, and Tunable Laser Systems

CNF Project Number: 3041-22

Principal Investigator(s): Adam Heiniger

User(s): Mateus Corato Zanarella

Affiliation(s): TOPTICA Photonics Inc.

Primary Source(s) of Research Funding: Self-funded

Contact: Adam.Heiniger@toptica-usa.com, mateus.corato.zanarella@toptica-usa.com

Research Group Website: https://www.toptica.com/

Primary CNF Tools Used: AJA Sputter, DISCO Dicing Saw, Hamatech Hot Piranha, Heidelberg DWL2000, JEOL JBX-9500FS E-beam Lithography System, KLA P7 Profilometer, MOS Clean Bench & Tanks, MRL B3 LPCVD LTO, MRL B4 LPCVD Nitride, MRL E4 LPCVD CMOS Nitride, Oxford 100 ICP Dielectric, Oxford 80 RIE, PT Takachi HDP-CVD, Suss MA6|BA6 Aligner, Unaxis 770 Deep Silicon Etch, YES EcoClean Asher, YES Asher, Zeiss Ultra SEM, Woollam RC2 Spectroscopic Ellipsometer, Keyence VHX-7100 Digital Microscope

Abstract:

As quantum technologies transition from laboratories to the world, their successful deployment critically relies on the size, weight, and power (SWaP) of the laser sources fueling them. Due to the stringent optical requirements of most of these systems, they still predominantly use bulky lasers made of free-space components. With the emergence of high-performance, chip-scale lasers based on photonic integrated circuits (PICs) [1], practical quantum systems that are compact and scalable are now within reach. However, to successfully realize a PIC-based laser module that meets both optical and functional requirements, a system-level approach for co-designing the optical source (gain medium and PIC), the driver electronics, and the control software needs to be adopted.

Summary of Research:

Our research comprises the design, fabrication, characterization, and packaging of PIC-based laser systems. The PIC components include the laser external cavity and any other desired light processing units to manipulate and deliver the light.

Conclusions and Future Steps:

We have successfully demonstrated a complete and compact PIC-based laser system around 780 nm wavelength targeting quantum applications. Our work was featured in the conference publications listed in References [2-4]. Future steps include improving the current system, expanding to other wavelengths, and adding more optical components for light manipulation and delivery.

- M. Corato-Zanarella, A. Gil-Molina, X. Ji, M. Chul Shin, A. Mohanty, M. Lipson, "Widely tunable and narrow-linewidth chip-scale lasers from near-ultraviolet to near-infrared wavelengths," Nat. Photon. 17, 157–164 (2023).
- [2] M. Corato-Zanarella, M. Lommel, D. Mayzlin, J. Nojic, A. Eras, C. Nölleke, B. Globisch, C. Haimberger, "Low-SWaP, Narrow-Linewidth, and Tunable Laser System For The Next Generation Of Quantum Technologies", 2025 Conference on Lasers and Electro-Optics Europe & European Quantum Electronics Conference (CLEO/Europe-EQEC), Munich, Germany (2025).
- [3] J. Nojic, A. Eras, L. Winkler, D. Mayzlin, M. Corato-Zanarella, M. Lommel, C. Nölleke, "Narrow-linewidth, Fully Integrated Chip-based Laser System in the Red Spectral Range", 2025 Conference on Lasers and Electro-Optics Europe & European Quantum Electronics Conference (CLEO/ Europe-EQEC), Munich, Germany (2025).
- [4] S. Dadras, M. Corato-Zanarella, A. Heiniger, C. Haimberger, "PIC-based tunable diode lasers for fieldable quantum applications", Proc. SPIE PC13563, Photonics for Quantum 2025, PC1356314 (18 July 2025); https://doi. org/10.1117/12.3065992.ff

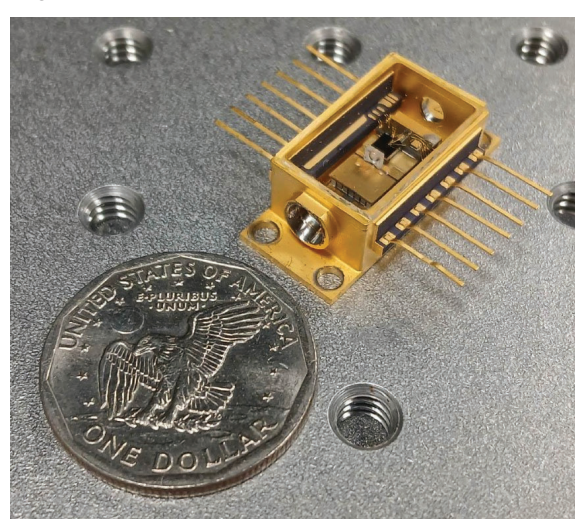


Figure 1: Low-SWaP, PIC-based laser.

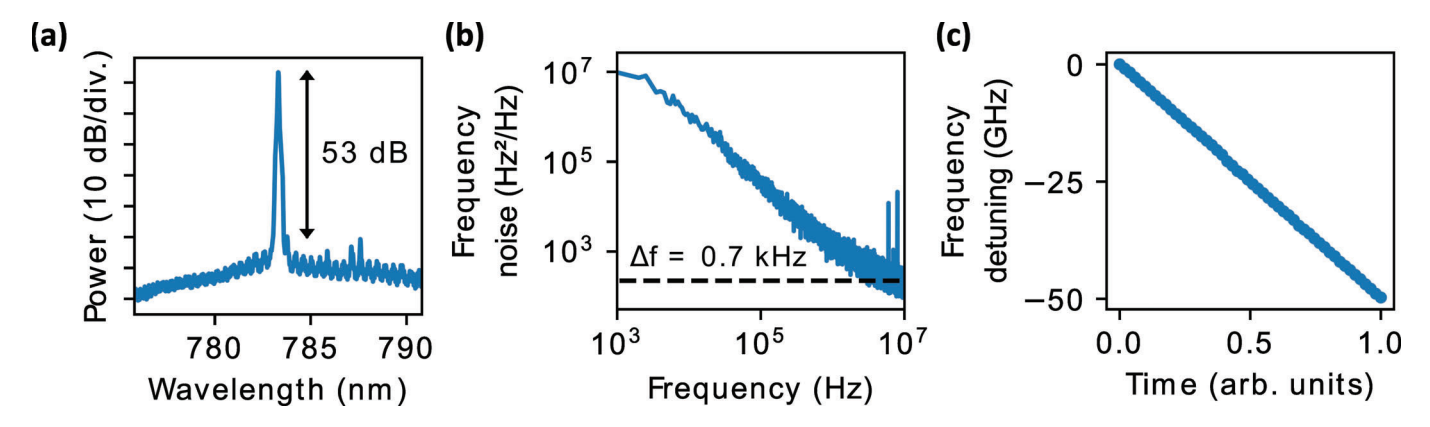


Figure 2: Example performance metrics of a PIC-based laser. (a) Side-mode suppression ratio. (b) Frequency noise. (c) Mode hop-free tuning range.

Design and Fabricate Robust Nanocavities

CNF Project Number: 3261-25 Principal Investigator(s): Wei Bao

User(s): Wei Li, Yilin Meng

Affiliation(s): Department of Materials Science and Engineering, Rensselaer Polytechnic Institute

Primary Source(s) of Research Funding: Army Research Office Contact: baow2@rpi.edu, liw24@rpi.edu, mengy5@rpi.edu Primary CNF Tools Used: Heidelberg MLA 150 Maskless Aligner

Summary of Research:

To realize tunable mid-infrared nanophotonic platforms with strong light–matter interaction, we are fabricating arrays of gold disks as the foundational step toward constructing epsilon-near-zero (ENZ) plasmonic nanocavities. As illustrated in Fig. 1a and 1b [Nat. Photonics 15, 125–130 (2021)], such nanocavities enable significant optical resonance and ultra-strong coupling with phonons. Gold is chosen as the cavity material due to its low intrinsic loss and chemical stability in the infrared range.

At Cornell CNF, we first spin-coated a UV photoresist and employed photolithography to define the gold disk array patterns. The primary lithography tool used was the Heidelberg MLA 150 Maskless Aligner. Subsequent processing was carried out at RPI, where we deposited a 3 nm titanium (Ti) adhesion layer followed by 100 nm gold (Au) using electron-beam evaporation. A standard lift-off process was then applied to form the final gold disk array. Characterization at RPI confirmed the fabrication results of the designed structures, as shown in Fig. 2a. The fabricated array features a periodicity of 4.77 μm and disk diameters of 1.76 μm. To evaluate the optical performance of the fabricated nanocavity structure, we conducted transmission measurements of

the bare gold disk array. The resulting spectrum (Fig. 2b) demonstrates an optical resonance, showing that our lithography created the intended plasmonic modes. However, the observed quality factor of the resonance remained low, suggesting the presence of optical loss. Further investigation using scanning electron microscopy (SEM), as shown in Fig. 2c, revealed prominent lift-off wings around the edge of each disk, which, we believe, are responsible for the elevated loss.

To address this issue, our next fabrication iteration will adopt a bilayer resist strategy to promote clean undercut profiles and facilitate lift-off process.

Conclusions and Future Steps:

The plasmonic disk array has been successfully fabricated, but the observed optical modes exhibit high loss, likely due to lift-off artifacts. Moving forward, we plan to use ASML PAS 5500/300C DUV Wafer Stepper and Heidelberg MLA 150 Maskless Aligner to optimize our fabrication. With high-quality plasmonic resonance mode achieved, we will coat the structure with ENZ materials to investigate cavity—matter coupling and explore optical control of material excitations.

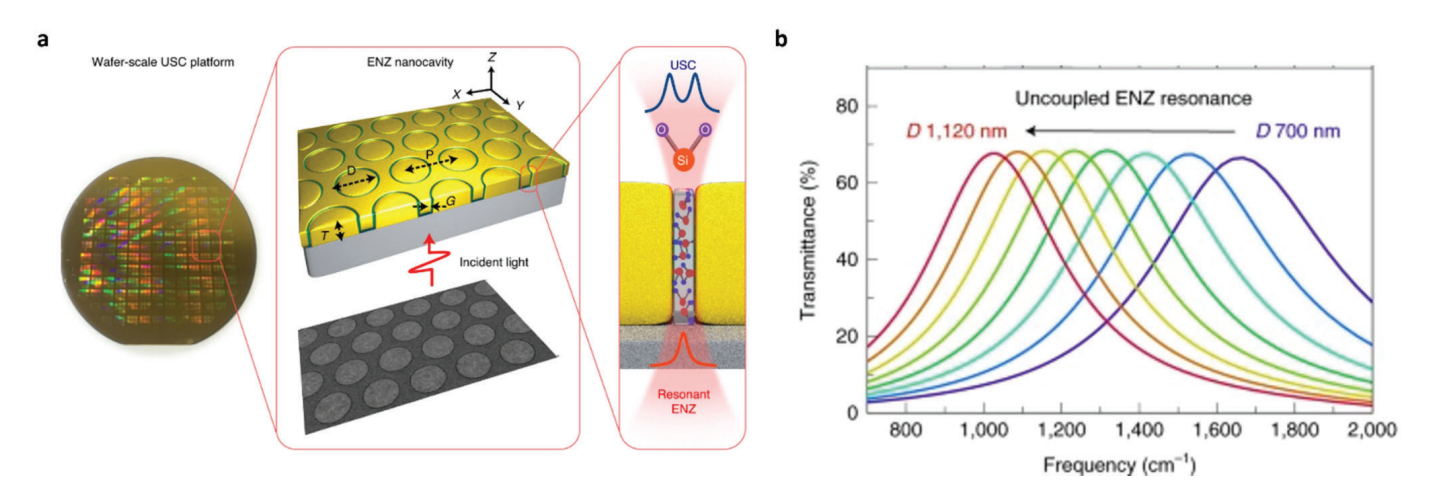


Figure 1: (a) Schematic of ENZ nanocavity and illustration of SiO2 phonons interacting with the nanocavity mode. (b) Transmission resonances of ENZ nanocavity with different aperture diameters. Image reproduced from Nat. Photonics 15, 125–130 (2021).

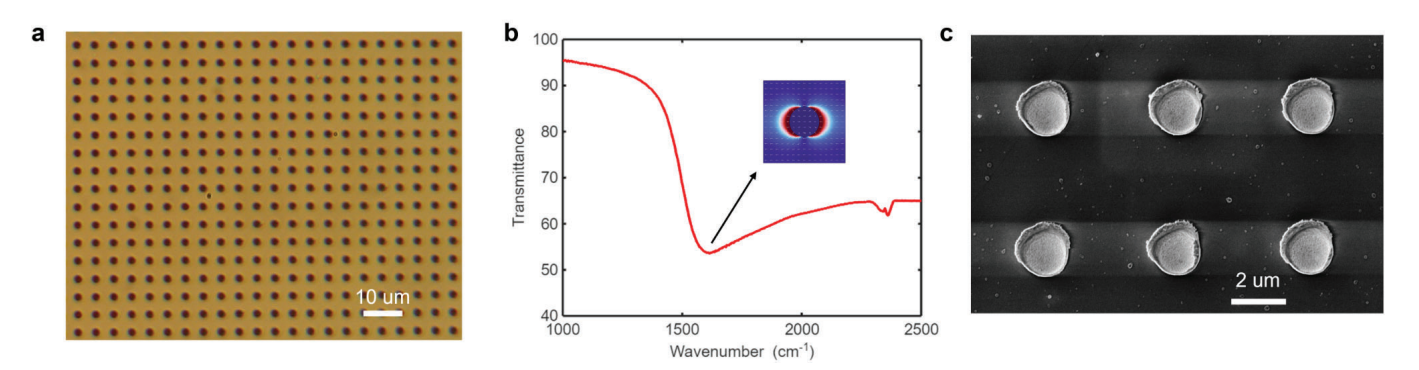


Figure 2: (a) Optical image of the fabricated gold disk array with a designed periodicity of 4.77 μ m and disk diameters of 1.76 μ m. (b) Measured transmission spectrum of the array, showing a resonance dip. The inset displays a simulated electric field profile of the resonance mode, indicating the dipolar resonance around the gold disk. (c) Scanning electron microscopy image reveals the presence of lift-off wings surrounding each gold disk.